Int. J. Heat Mass Transfer. Vol. 31, No. 2, pp. 387–396, 1988
Printed in Great Britain

0017–9310/88 $3.00+0.00

Laminar heat transfer in a helically coiled tube

KOZO FUTAGAMI and YOSHIYUKI AOYAMA
Department of Mechanical and Industrial Engineering, Faculty of Engineering,
Ehime University, Matsuyama, Ehime, Japan

(*Received* 1 *September* 1987)

Abstract—A theoretical and experimental study is carried out on the effect of the secondary flow on heat transfer from a uniformly heated helically coiled tube to fully developed laminar flow. Both the centrifugal and buoyancy forces are taken into account in the numerical analysis. The solutions cover a wide range of Prandtl numbers. The velocity and temperature profiles, the friction factor and heat transfer coefficient are obtained. The effects of the secondary flow on heat transfer are divided into three types: those in the centrifugal, the buoyant and the composite range; and the boundaries are determined. An approximate expression for the peripherally averaged Nusselt number in the composite range is given as a function of two simple factors. A comparison is made with the results of the experiments using water. The effect of the inclination of the tube is discussed.

1. INTRODUCTION

HEAT EXCHANGERS equipped with a helically coiled tube are used in various fields of industry, but forced convective heat transfer in a tube of this type has not been adequately studied.

Many experimental and theoretical papers [1–8] have reported on convective heat transfer in a circularly curved tube. It has been made clear that the secondary flow resulting from the centrifugal force causes the heat transfer coefficient to be significantly higher than that in a straight tube. The secondary flow is also induced due to the buoyancy force, even in the straight tube placed horizontally or inclined, unless the temperature gradient in a cross section of the tube is negligible [9, 10].

In the helically-coiled-tube heat exchanger, the secondary flow is induced mainly by the centrifugal force (centrifugal range), the buoyancy force (buoyant range), or by both (composite range), according to operating conditions. The criterion for the conditions that distinguish these ranges has been reported by some investigators [11–13]. Prusa and Yao [12] provided a flow-regime map for a Prandtl number of unity, and Lee *et al.* [13] showed a similar map. These maps are based on the results of the numerical analyses. Singh and Bell [14] presented an empirical expression for the heat transfer coefficient in the composite range, but their data scatters widely around the expression.

This paper mainly describes a theoretical study on the effect of the secondary flow on heat transfer from a uniformly heated helically coiled tube to a fully developed laminar flow. Both the centrifugal force and the buoyancy force are introduced in the governing equations. Numerical analysis is extended to cover a region with higher Prandtl numbers than those in the previous work by the authors [15]. The velocity and temperature profiles, the friction factor and the heat transfer coefficient are obtained in the composite range, and the boundaries of the composite range are expressed by simple relations of two parameters. A comparison is made with the results of the experiments using water. The effect of the inclination of the tube axis is discussed.

2. THEORY AND NUMERICAL ANALYSIS

2.1. *Coordinate system and governing equations*

The system of coordinates used in this analysis is shown in Fig. 1. The tube axis is inclined at angle α with the horizontal plane (the x–y plane). Point A lies on the tube axis. Coordinate θ is defined as the angle between 0A and 0x, and r and ϕ are the radial and angular coordinates taken in the circular cross section perpendicular to the tube axis. Point A′ is the projection of A on the x–y plane. The angle θ^* is that between 0x and 0A′. Thus, the transformation from rectangular coordinates (x, y, z coordinates) to curvilinear coordinates (r, ϕ, θ coordinates) is given as

$$x = (R+r\cos\phi)\cos\theta^* + r\sin\phi\sin\alpha\sin\theta^* \quad (1)$$

$$y = (R+r\cos\phi)\sin\theta^* - r\sin\phi\sin\alpha\cos\theta^* \quad (2)$$

$$z = R\theta^*\tan\alpha + r\sin\phi\cos\alpha. \quad (3)$$

The following assumptions are made.

(1) The fluid flow is steady, and hydrodynamically and thermally fully developed.

(2) The density variation is considered in the buoyancy term alone, and the other physical properties are constant.

(3) The wall heat flux is uniform.

(4) The radius of the tube is very small in comparison with the coil radius, that is, $a/R \ll 1$.

(5) Heat conduction in the direction of the tube axis

NOMENCLATURE

a	tube radius
De	Dean number, $Re\sqrt{(a/R)}$
g	gravitational acceleration
h	heat transfer coefficient
L	distance from the start of heating
Nu	Nusselt number, $2ah/\lambda$
Nu_b	Nusselt number in the case where the buoyancy force alone acts
Nu_c	Nusselt number in the case where the centrifugal force alone acts
Nu_ϕ	peripheral local Nusselt number
Nu_0	Nusselt number for Poiseuille flow, 48/11
P	pressure
Pr	Prandtl number, ν/κ
q	heat flux
R	radius of the coil
Ra	Rayleigh number, $g\beta\tau a^4/\kappa\nu$
Re	Reynolds number, $2aw_m/\nu$
r, ϕ, θ	coordinates
r^*	dimensionless radial coordinate, r/a
T	local temperature
T_m	mixed mean temperature
T_w	wall temperature
T^*	dimensionless temperature, $(T_w-T)/\tau a\, Re\, Pr$
δT	temperature difference, $T-T_w$
u, v, w	velocity components in the r, ϕ and θ directions
u^*, v^*, w^*	components of the dimensionless velocity defined by equation (17)
Z	$L/2a$.

Greek symbols

α	inclination angle of the tube axis
β	volumetric thermal expansion coefficient
Δ	Laplacian operator, $\partial^2/\partial r^2+(1/r)\partial/\partial r+(1/r^2)\partial^2/\partial\phi^2$
Δ^*	dimensionless Laplacian operator, see equation (16)
κ	thermal diffusivity
λ	thermal conductivity
Λ	friction factor, see equation (10)
ν	kinematic viscosity
ξ^*	dimensionless vorticity, $\Delta^*\psi^*$
ρ	density
τ	axial temperature gradient
ψ	stream function
ψ^*	dimensionless stream function, ψ/ν.

Subscripts

c	center
0	Poiseuille flow.

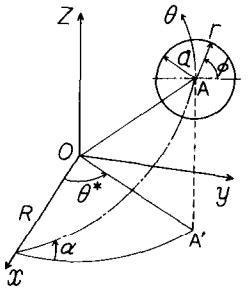

FIG. 1. The coordinate system.

is neglected, and the peripheral wall temperature is uniform.

Employing the curvilinear coordinates explained above and taking into account the above assumptions yield the following continuity, momentum and energy equations:

$$\frac{\partial u}{\partial r}+\frac{u}{r}+\frac{1}{r}\frac{\partial v}{\partial \phi}=0 \tag{4}$$

$$u\frac{\partial u}{\partial r}+\frac{v}{r}\frac{\partial u}{\partial \phi}-\frac{v^2}{r}-\frac{\cos^2\alpha\cos\phi}{R}w^2 = -\frac{1}{\rho}\frac{\partial p}{\partial r}+\nu\left(\Delta u-\frac{u}{r^2}-\frac{2}{r^2}\frac{\partial v}{\partial \phi}\right)+\beta(\delta T)g\cos\alpha\sin\phi \tag{5}$$

$$u\frac{\partial v}{\partial r}+\frac{v}{r}\frac{\partial v}{\partial \phi}+\frac{uv}{r}+\frac{\cos^2\alpha\sin\phi}{R}w^2 = -\frac{1}{\rho r}\frac{\partial p}{\partial \phi}+\nu\left(\Delta v-\frac{v}{r^2}+\frac{2}{r^2}\frac{\partial u}{\partial \phi}\right)+\beta(\delta T)g\cos\alpha\cos\phi \tag{6}$$

$$u\frac{\partial w}{\partial r}+\frac{v}{r}\frac{\partial w}{\partial \phi}=-\frac{\cos\alpha}{\rho R}\frac{\partial p}{\partial \theta^*}+\nu\Delta w+\beta(\delta T)g\sin\alpha \tag{7}$$

$$u\frac{\partial T}{\partial r}+\frac{v}{r}\frac{\partial T}{\partial \phi}+\frac{w\cos\alpha}{R}\frac{\partial T}{\partial \theta^*}=\kappa\Delta T \tag{8}$$

where u, v and w are the radial, peripheral and axial components of the fluid velocity, p, ρ and β are the pressure, density and volumetric thermal expansion coefficients of the fluid, respectively, and δT is the temperature difference, $T-T_w$.

The peripherally averaged Nusselt number Nu and friction factor Λ are defined by

$$Nu=\frac{2qa}{\lambda(T_w-T_m)} \tag{9}$$

$$\Lambda=\frac{-4a\cos\alpha}{\rho w_m^2}\frac{dp}{R\,d\theta^*} \tag{10}$$

where q, T_w, T_m, w_m and λ are the wall heat flux, wall temperature, mixed mean temperature, mean axial

velocity and thermal conductivity of the fluid, respectively.

Upon eliminating the pressure terms in equations (5) and (6), and introducing the stream function ψ and the vorticity of the secondary flow ξ, the governing equations are rewritten in dimensionless form as follows:

$$u^* = \frac{1}{r^*}\frac{\partial \psi^*}{\partial \phi}, \quad v^* = -\frac{\partial \psi^*}{\partial r^*} \tag{11}$$

$$\xi^* = \Delta^* \psi^* \tag{12}$$

$$u^*\frac{\partial \xi^*}{\partial r^*} + \frac{v^*}{r^*}\frac{\partial \xi^*}{\partial \phi} = \Delta^*\xi^* + \tfrac{1}{2}De^2\cos^2\alpha\left(\frac{\partial w^*}{\partial r^*}\sin\phi + \frac{\partial w^*}{r^*\partial\phi}\cos\phi\right) - Re\,Ra\cos\alpha\left(\frac{\partial T^*}{r^*\partial\phi}\sin\phi - \frac{\partial T^*}{\partial r^*}\cos\phi\right) \tag{13}$$

$$u^*\frac{\partial w^*}{\partial r^*} + \frac{v^*}{r^*}\frac{\partial w^*}{\partial \phi} = \Delta^* w^* - \frac{Re}{2}\frac{\cos\alpha}{R^*}\frac{\partial p^*}{\partial \theta^*} - 2Ra\,T^*\sin\alpha \tag{14}$$

$$Pr\left(u^*\frac{\partial T^*}{\partial r^*} + \frac{v^*}{r^*}\frac{\partial T^*}{\partial \phi}\right) = \Delta^* T^* + \tfrac{1}{2}w^* \tag{15}$$

where

$$\Delta^* = \frac{\partial^2}{\partial r^{*2}} + \frac{1}{r^*}\frac{\partial}{\partial r^*} + \frac{1}{r^{*2}}\frac{\partial^2}{\partial \phi^2} \tag{16}$$

$$r^* = \frac{r}{a}, \quad R^* = \frac{R}{a}, \quad u^* = \frac{au}{\nu}, \quad v^* = \frac{av}{\nu}, \quad w^* = \frac{w}{w_m} \tag{17}$$

$$T^* = \frac{T_w - T}{\tau a\, Re\, Pr}, \quad p^* = \frac{p}{\rho w_m^2}, \quad \psi^* = \frac{\psi}{\nu}, \quad \xi^* = \frac{a^2}{\nu}\xi.$$

The dimensionless parameters *Re*, *Ra*, *De* and *Pr* are the Reynolds, Rayleigh, Dean and Prandtl numbers, respectively.

Equations (9) and (10) can be rewritten as

$$Nu = \frac{1}{2T_m^*} \tag{18}$$

$$\Lambda = \frac{-4\cos\alpha}{R^*}\frac{dp^*}{d\theta^*}. \tag{19}$$

The boundary conditions can be written as

$$w^* = T^* = \psi^* = 0, \quad \xi^* = \partial^2\psi^*/\partial r^{*2} \quad \text{at} \quad r^* = 1$$
$$w^*, T^*, \psi^*, \xi^* \quad \text{are finite at } r^* = 0. \tag{20}$$

The centrifugal and buoyancy contributions are contained in the second and third terms on the right-hand side of equation (13), namely, the momentum equation for the secondary flow. The third term on the right-hand side of equation (14) represents the effect of the component of the buoyancy force in the direction of the tube axis.

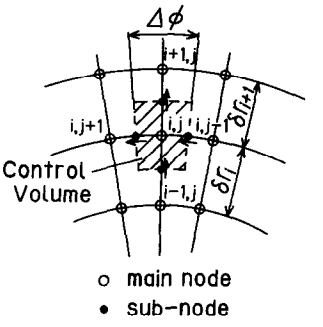

FIG. 2. Numerical grids and control volume.

2.2. *Numerical method and computational procedure*

Equations (13)–(15) become the unsteady-state equations by adding the time derivatives of ξ^*, w^* and T^*, respectively. Then, the control volume approach is used to derive the finite-difference equations. The steady-state solution is obtained as an asymptotic solution of this unsteady system of equations. Figure 2 shows the mesh system and a control volume for the numerical calculation. Each surface of the control volume exists at the midpoint between the main nodes across a grid axis. The radial velocity u or the ϕ-component v is calculated at the subnode on the surface. The direction of the velocity is perpendicular to the surface. The upwind difference is applied to the convection term. This discretization concept is equivalent to the tank and tube concept by Gosman *et al.* [16].

The radial and angular coordinates are divided into 20 and 26 intervals, respectively (henceforth, this grid size is represented by 20×26). The grid spacing is equal in the ϕ-direction. In the r-direction it is unequal, since $\delta r_i/\delta r_{i+1} = 1.1$. This grid size was chosen after some calculations were tried with 30×34 and 40×26 mesh systems ($\delta r_i/\delta r_{i+1} = 1.02$). The boundary condition, equation (20), is converted into

$$w^* = T^*_{N,j} = \psi^*_{N,j} = 0, \quad \xi^*_{N,j} = 3\frac{\psi^*_{N-1,j}}{\delta r_N^2} - 0.5\xi^*_{N-1,j}. \tag{21}$$

The value of boundary vorticity is estimated by the second-order form [17, 18]. The governing equations (11)–(15) cannot be used at the center because of their singularities. Therefore, equations (14) and (15) are written with the Cartesian coordinates at the center. Stream function and vorticity are obtained by averaging the values at all the neighboring grids.

There are two alternative expressions for Nusselt number. One, which already has been given as equation (18), is obtained from the energy balance in the direction of the tube axis. This Nusselt number is denoted by Nu_1. Another is obtained based on the temperature gradient at the tube wall, and is denoted by Nu_2. Thus, one obtains

$$Nu_2 = \frac{-\int_0^{2\pi}\left(\frac{\partial T^*}{\partial r^*}\right)_{r^*=1} d\phi}{\pi T_m^*}. \tag{22}$$

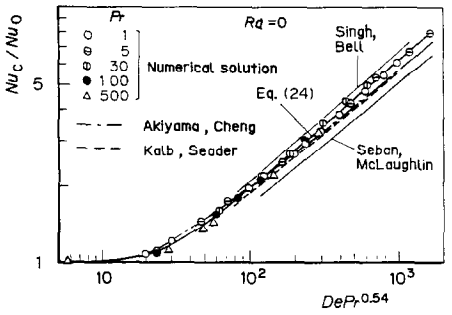

FIG. 3. Dependence of the Nusselt number on $De\,Pr^{0.54}$ for $Ra = 0$.

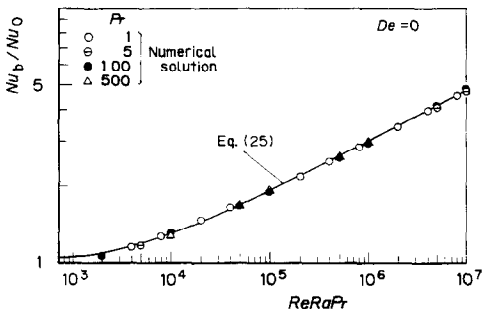

FIG. 4. Dependence of the Nusselt number on $Re\,Ra\,Pr$ for $De = 0$.

The mean value of Nu_1 and Nu_2 is adopted as the peripherally averaged Nusselt number Nu. The difference between Nu_1 and Nu_2 is concerned with the accuracy of the numerical solution. The relative difference $|Nu_1 - Nu_2|/Nu_1$ is less than 0.03 in this calculation.

An implicit scheme is used at each time step, and converged solutions are obtained by iteration. Actually, several iterations are executed, since this procedure does not require fully convergent values at each step. Arriving at the steady-state condition, only one iteration is enough to satisfy the following error criterion:

$$\max(|F^{n+1} - F^n|/|F^{n+1}|) < 10^{-5}. \qquad (23)$$

2.3. *Numerical results and discussion*

2.3.1. *Numerical results for* $\alpha = 0$. Figure 3 shows Nu_c/Nu_0 against $De\,Pr^{0.54}$, where Nu_c denotes the Nusselt number for $Ra = 0$ and Nu_0 is the Nusselt number for Poiseuille flow in a straight tube. Since the secondary flow is induced only by the centrifugal force, the Nusselt number can be expressed as a function of Dean and Prandtl numbers. It can be seen that Nu_c/Nu_0 is well correlated with $(De\,Pr^{0.54})^{0.5}$. Thus, a correlation is derived as

$$\left(\frac{Nu_c}{Nu_0}\right)^6 = 1 + [0.195(De\,Pr^{0.54})^{0.5}]^6. \qquad (24)$$

The power of the Dean number is equal to Mori and Nakayama's [1] theoretical result using the boundary layer approximation. Numerical results obtained by Akiyama and Cheng [3] and Kalb and Seader [6] are also shown for $Pr = 1$ in Fig. 3. Experimental results for the various Prandtl numbers given by Singh and Bell [14], and given by Seban and McLaughlin [2] are drawn. Singh and Bell's results are for $a/R = 41.7$ and $Pr = 100$, whereas they reported a little dependence upon coil geometry a/R. Seban and McLaughlin reported $Nu_{\phi\,\max}$ and $Nu_{\phi\,\min}$, which were obtained at the outer and inner tube walls, respectively. We have used their mean values, assuming $Pr = 100$. Seban and McLaughlin's result is lower than our correlation. However, this discrepancy is not necessarily significant, since the mean value $(Nu_{\phi\,\max} + Nu_{\phi\,\min})/2$ is less than the peripherally averaged Nusselt number by a factor of 0.8 (Fig. 8(a)).

Figure 4 shows the variation of Nu_b/Nu_0 with $Re\,Ra\,Pr$, where Nu_b is the Nusselt number when $De = 0$. Secondary flow is induced only by the buoyancy force. Eventually, the Nusselt number is equal to that in the heated straight tube. Applying the boundary layer approximation, Mori and Futagami [19] had a result that the Nusselt number was proportional to $(Re\,Ra)^{0.2}$ in the large $Re\,Ra$ region. Now we propose the following correlation which is applicable in the whole $Re\,Ra\,Pr$ region:

$$\left(\frac{Nu_b}{Nu_0}\right)^{4.5} = 1 + [0.19(Re\,Ra\,Pr)^{0.2}]^{4.5}. \qquad (25)$$

Our results agree well with the numerical results given by Hwang and Cheng [9].

Some computed streamlines for secondary flow, isotherms and isometries of the axial velocity are shown in Fig. 5 for $Pr = 1$ and in Fig. 6 for $Pr = 100$. The value of $Re\,Ra\,Pr$ increases from (a) to (c) with $De\,Pr^{0.54}$ kept constant. In the case of $Ra = 0$ (Figs. 5(a) and 6(a)), only the centrifugal force is induced. Therefore, streamlines, etc. are symmetrical with respect to the horizontal centerline. They rotate clockwise as Ra increases and the buoyancy effect becomes significant. As $Re\,Ra\,Pr$ becomes much larger, they tend to be symmetrical with respect to the vertical centerline.

The profiles of the streamlines, etc. are also dependent on the Prandtl number. If $Pr = 1$, the isometry of $\psi^* = 0$ remains a straight line in the rotating process mentioned above. However, in the case of $Pr = 100$, it is distorted near the stagnation point where the secondary flow strikes the tube wall. The low-temperature region, where the magnitude of the dimensionless temperature is large, exists in the vicinity of the outer wall for $Ra = 0$ and $Pr = 1$ (Fig. 5(a)). This region moves clockwise with increasing $Re\,Ra\,Pr$. For $Pr = 100$, if $Ra = 0$, two low-temperature regions (large dimensionless temperature) exist separately near the centers of the upper and lower halves. The upper low-temperature region disappears as $Re\,Ra\,Pr$ is increased. The low-temperature region is located between $\phi = \pi$ and $3/2\pi$. The isotherms for $Pr = 100$ are greatly skewed compared with those for $Pr = 1$.

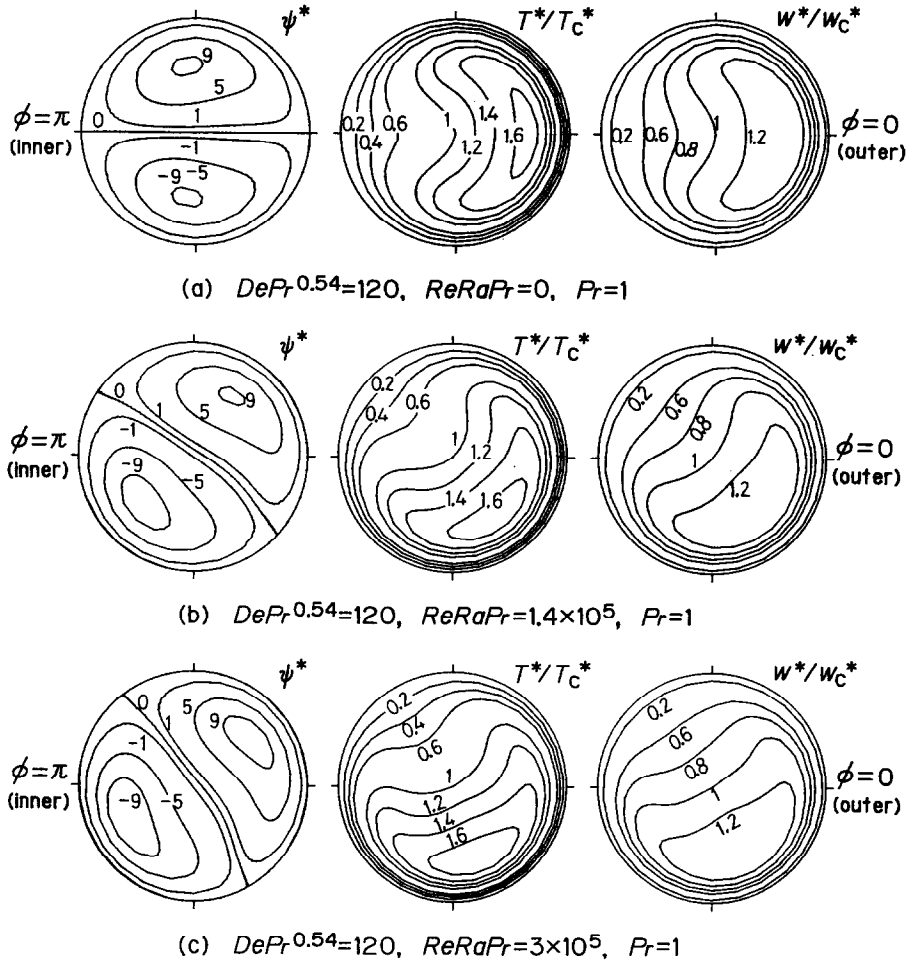

FIG. 5. Streamlines for secondary flow (on the left), isotherms (in the middle) and isometries of the axial velocity (on the right); $Pr = 1$.

Figures 7 and 8 show the peripheral variations of the relative local Nusselt number Nu_ϕ/Nu_0. The angle at the maximum and minimum of Nu_ϕ/Nu_0 is 0 and π for $Ra = 0$, respectively. These points rotate clockwise as $Re\,Ra\,Pr$ is increased. In the case of $Pr = 1$, the profile remains almost symmetrical with respect to the $Nu_{\phi\,\max}$–$Nu_{\phi\,\min}$ line, even if rotation occurs. However, for $Pr = 100$, the symmetrical profile cannot be seen. The magnitude of the rotation for $Nu_{\phi\,\max}$ is greater than that for $Nu_{\phi\,\min}$.

Figure 9 shows the variation of the friction factor with De and $Re\,Ra$. Our results agree well with Ito's correlation [20] for $Ra = 0$ where the buoyancy force is absent. Ito's correlation is an asymptotic one to which the friction factor should approach as the Dean number increases, that is, the buoyancy force becomes less effective. If the Dean number decreases, then the buoyancy force becomes dominant, and, consequently, the friction factor becomes a function of $Re\,Ra$ alone. Therefore, if the value of $Re\,Ra$ is constant, another asymptotic correlation should be $\Lambda/\Lambda_0 = \text{const}$. In Fig. 9, a transitional region can be seen between these two asymptotes. Both the centrifugal and buoyancy forces are effective in this region. It can also be seen that Λ/Λ_0 in the transitional region is larger than that for $Ra = 0$ and that for $De = 0$.

Figure 10 shows Nu/Nu_0 against $De\,Pr^{0.54}$ with $Re\,Ra\,Pr$ as a parameter. If $De\,Pr^{0.54}$ becomes smaller, the Nusselt number has an asymptotic value dependent only on $Re\,Ra\,Pr$. This asymptotic value has been given by equation (25). On the other hand, with increasing Dean number, Nu/Nu_0 tends to approach the value calculated from equation (24). The transitional region exists for the Nusselt number as well as the friction factor. The above result is well approximated by the following correlation in the whole range of $De\,Pr^{0.54}$

$$\frac{Nu}{Nu_0} = 1 + \left[\left(\frac{Nu_c}{Nu_0} - 1\right)^4 + \left(\frac{Nu_b}{Nu_0} - 1\right)^4\right]^{1/4}. \quad (26)$$

Now, it is useful to obtain the boundaries of the following three ranges: (a) the centrifugal force is dominant; (b) both the centrifugal and buoyancy forces are effective (composite range); (c) the buoyancy

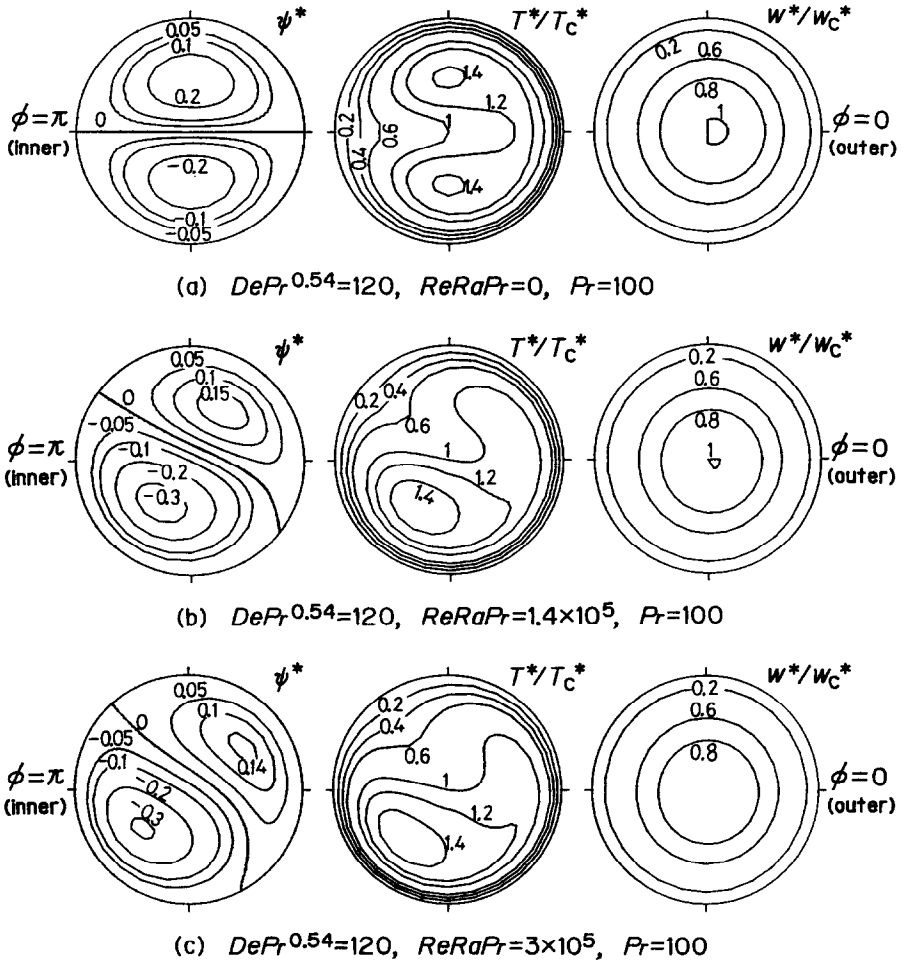

FIG. 6. Streamlines for the secondary flow (on the left), isotherms (in the middle) and isometries of the axial velocity (on the right); $Pr = 100$.

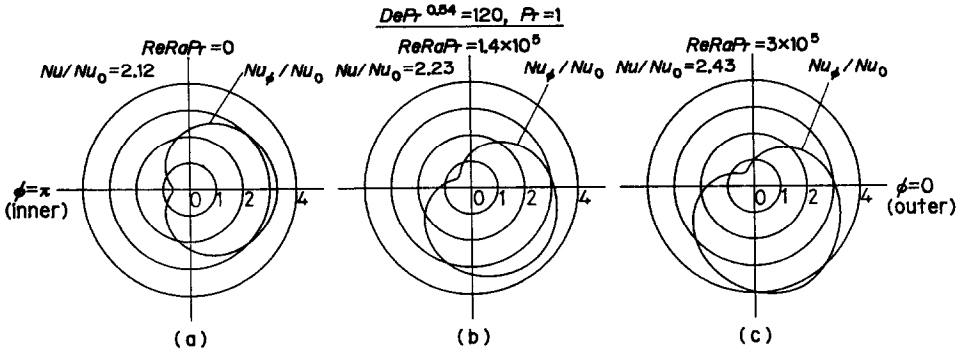

FIG. 7. Distributions of the relative peripheral local Nusselt numbers ($Pr = 1$).

force is dominant. The transitional region in the previous paragraphs is the same as the composite range. Boundary B1 is that which divides ranges (a) and (b), and B2 is the boundary which divides (b) and (c). As seen from Fig. 10, there are no obvious distinctions between the two neighboring ranges. Therefore, the authors define these boundaries by

$$|Nu_{\text{comp}} - Nu_{\text{mono}}|/Nu_{\text{mono}} = 0.02 \qquad (27)$$

where the subscript 'mono' means the range where either force is dominant, and the subscript 'comp' means the composite range.

The points on boundary B1 are plotted in Fig. 11, and the points on boundary B2 in Fig. 12. The equa-

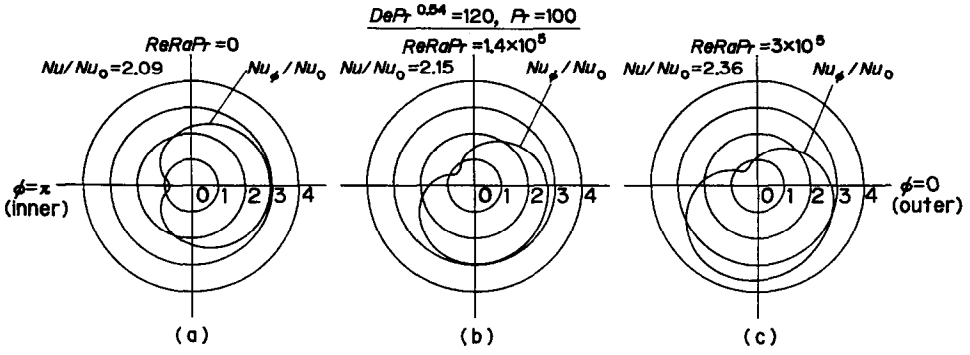

FIG. 8. Distributions of the relative peripheral local Nusselt numbers (Pr = 100).

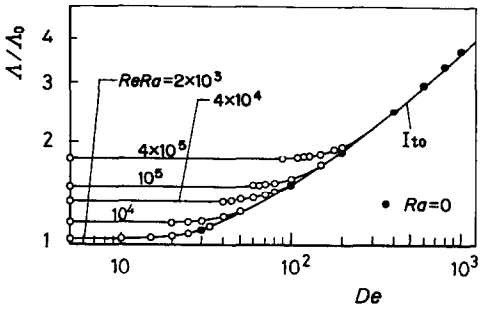

FIG. 9. Dependence of the relative friction factor on De with $Re\,Ra$ as a parameter.

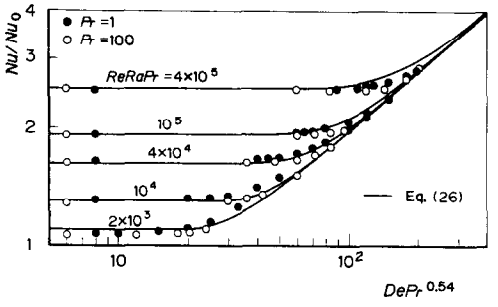

FIG. 10. Dependence of the relative Nusselt number on $De\,Pr^{0.54}$ with $Re\,Ra\,Pr$ as a parameter.

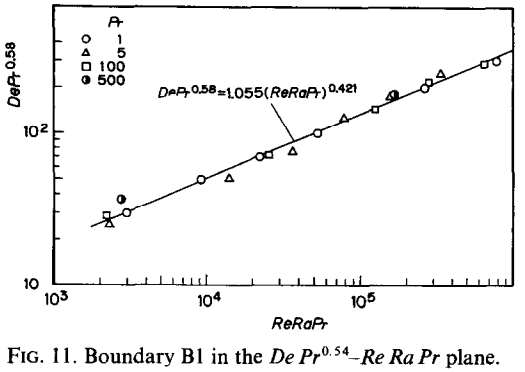

FIG. 11. Boundary B1 in the $De\,Pr^{0.54}$–$Re\,Ra\,Pr$ plane.

tions representing the boundaries can be obtained by the least-squares method as follows:

$$\text{B1:}\quad De\,Pr^{0.58} = 1.055(Re\,Ra\,Pr)^{0.421} \qquad (28)$$

$$\text{B2:}\quad De\,Pr^{0.5} = 0.8156(Re\,Ra\,Pr)^{0.386}. \qquad (29)$$

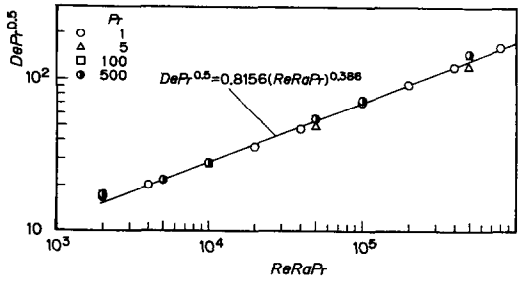

FIG. 12. Boundary B2 in the $De\,Pr^{0.54}$–$Re\,Ra\,Pr$ plane.

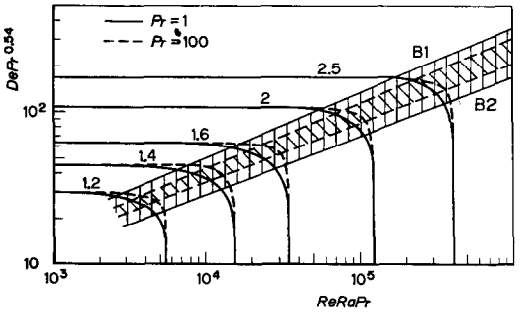

FIG. 13. A contour map showing the heat transfer ranges.

It is noted that the power of the Prandtl number is 0.58 and 0.5 on the left-hand side of equations (28) and (29), respectively. They are different from the power which has been used in equation (24).

A contour map showing the heat transfer ranges is shown in Fig. 13. $De\,Pr^{0.54}$ and $Re\,Ra\,Pr$ chosen as the axes are the same parameters as used in equations (24) and (25), respectively. Each contour in the figure has a horizontal asymptote on which the buoyancy force does not act, and it has a vertical asymptote on which the centrifugal force does not act. Boundaries B1 and B2 are drawn. The shaded area between them is the composite range. B1 and B2 are affected by the Prandtl number, and the composite range becomes narrow as Pr is increased. This result is caused by the difference in the power of Pr between $De\,Pr^{0.58}$ in equation (28) and $De\,Pr^{0.5}$ in equation (29).

It is of interest to know the angle at which the peripherally local Nusselt number Nu_ϕ has a maximum and minimum in the composite range.

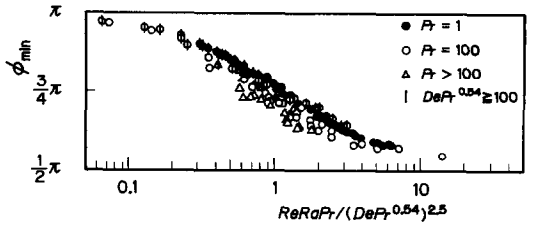

FIG. 14. Variation of the peripheral angle at which the peripheral local Nusselt number takes a minimum value.

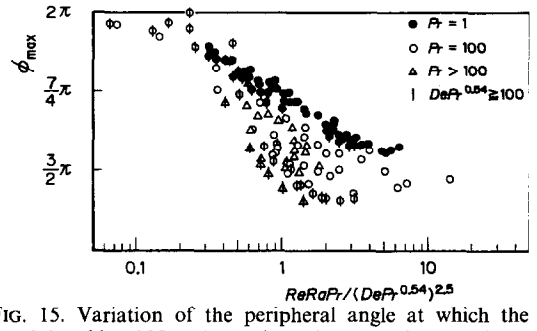

FIG. 15. Variation of the peripheral angle at which the peripheral local Nusselt number takes a maximum value.

These angles are denoted by ϕ_{max} and ϕ_{min}, respectively. Some examples of the distribution of Nu_ϕ are shown in Figs. 7 and 8.

As shown in Fig. 14, ϕ_{min} is represented as a function of $Re\ Ra\ Pr/(De\ Pr^{0.54})^{2.5}$. ϕ_{min} is equal to π (inner wall) when the buoyancy force does not act, and decreases to $\pi/2$ (top) as it becomes significant. As for $Pr = 1$, ϕ_{min} correlates well with this parameter alone.

Figure 15 shows the variation of ϕ_{max}. ϕ_{max} is 2π (outer wall) when the buoyancy force is absent, and is asymptotic to 1.5π (bottom) as it becomes dominant. In the case of $Pr = 1$, ϕ_{max} can be fairly well correlated with $Re\ Ra\ Pr/(De\ Pr^{0.54})^{2.5}$ alone. Thus, ϕ_{max} is nearly opposite to ϕ_{min} as shown in Fig. 7. However, as Pr becomes large, ϕ_{max} cannot be a function of one parameter only. If $De\ Pr^{0.54}$ becomes larger, ϕ_{max} decreases to less than 1.5π and then increases to approach it.

2.3.2. *The effect of the inclination of the tube axis.* As estimated from equation (13) $De\cos\alpha$ and $Re\ Ra\cos\alpha$ should be used instead of De and $Re\ Ra$, respectively, in the case of $\alpha \neq 0$. Thus Nu/Nu_0 is shown in Fig. 16 against $De\ Pr^{0.54}\cos\alpha$ with $Re\ Ra\ Pr\cos\alpha$ as a parameter, where α and a/R are fixed as constants, namely, $\pi/4$ and 0.01, respectively. It seems that as De becomes smaller, the relative Nusselt number has a minimum and then continues to increase. However, this continuous increase is not due to the decrease in De, but to a resulting increase in Ra. If a/R, α and $Re\ Ra$ are constant, Ra increases as De and accordingly Re are decreased. The increase in Ra results in an increase in the third term on the right-hand side of equation (14) since α is positive, and causes the increase of the Nusselt number in the low De region.

It is of note that the third term of equation (14)

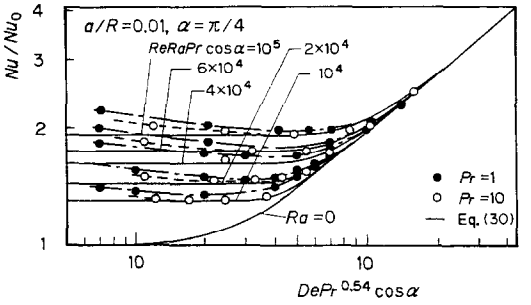

FIG. 16. The effect of the inclination on relative Nusselt number in a helically coiled tube ($\alpha = \pi/4$).

mentioned above represents the tube-axial component of the buoyancy force. In the case of $\alpha < 0$, the Nusselt number will decrease as De is decreased, since the axial component of the buoyancy force acts on the fluid against the axial flow and becomes relatively significant. Futagami and Abe [10] ascertained for an inclined straight tube where De was zero but Ra was finite that the Nusselt number decreased as the inclination angle became negative.

If $Re\ Ra\ Pr$ and $De\ Pr^{0.54}$ are constant, Ra decreases as Pr is increased, consequently, the relative Nusselt number for $Pr = 10$ takes a lower value than that for $Pr = 1$. The solid line in Fig. 16 is a plot of the following approximate equation:

$$\frac{Nu}{Nu_0} = 1 + \left[\left(\frac{Nu_c}{Nu_0} - 1\right)^4 + \left(\frac{Nu_b}{Nu_0} - 1\right)^4\right]^{1/4} \quad (30)$$

where

$$\left(\frac{Nu_c}{Nu_0}\right)^6 = 1 + [0.195(De\ Pr^{0.54}\cos\alpha)^{0.5}]^6 \quad (31)$$

$$\left(\frac{Nu_b}{Nu_0}\right)^{4.5} = 1 + [0.19(Re\ Ra\ Pr\cos\alpha)^{0.2}]^{4.5}. \quad (32)$$

Equation (30) is the same as equation (26) except that $De\cos\alpha$ and $Re\ Ra\cos\alpha$ are used in the expressions for Nu_c/Nu_0 and Nu_b/Nu_0 instead of De and $Re\ Ra$, respectively. This equation expressed well the relative Nusselt number at least in the centrifugal and composite ranges. As α decreases, equation (30) becomes valid even in the buoyant range. Usually, the inclination angle is less than $\pi/4$ in a practical heat exchanger. Therefore, equation (30) will be applicable in all the ranges. Equations (28) and (29) can be used to express boundaries B1 and B2 if De and $Re\ Ra$ are replaced by $De\cos\alpha$ and $Re\ Ra\cos\alpha$, respectively.

3. EXPERIMENTS

Experiments of heat transfer were performed with water under the conditions of constant heat flux and fully developed flow. The parameters ranged so as to cover the composite range.

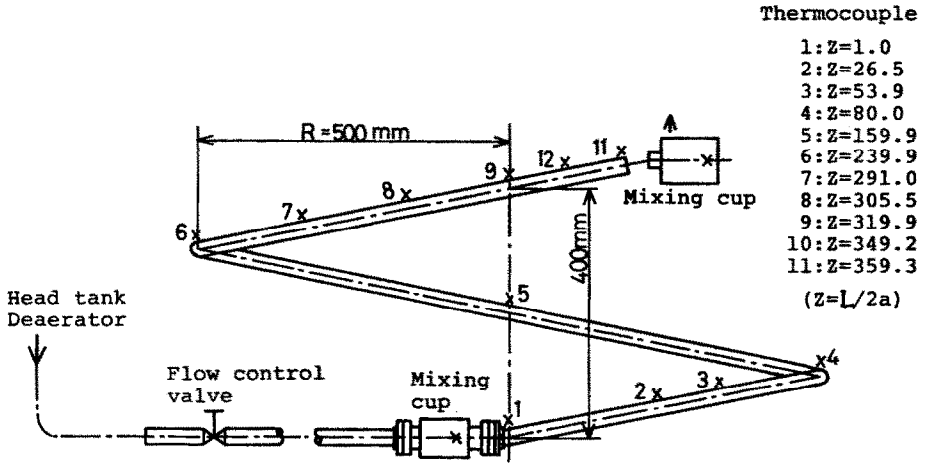

FIG. 17. A schematic diagram of the experimental apparatus.

3.1. *Apparatus and procedure*

Figure 17 shows the schematic diagram of the experimental apparatus. Water is supplied from the head tank. It flows through a deaerator, a flow control valve, an inlet mixing cup, a helically coiled tube and an outlet mixing cup before being discharged. The helically coiled tube was fabricated from a straight tube of copper with a devised bender, and hence, its cross-section was almost perfectly circular. The tube had a 9.9 mm i.d., a wall thickness of 1.2 mm and a length of 3.56 m. The diameter of the coil was 1 m; and therefore, $a/R = 1/101$. The inclined angle of the tube axis α was 0.12 rad (7°).

The tube was covered with thin asbestos for electrical insulation, on which nichrome wires were wound and used as an electrical heater. The outside was insulated with asbestos and glass wool. Inevitable heat loss was made uniform by increasing the thickness of glass wool toward the outlet. The tube was thermally insulated from the mixing cups.

The inlet and outlet temperatures were measured in the mixing cups with thermocouples 0.3 mm in diameter. Temperatures at the top of the tube wall were measured at the locations shown in Fig. 17. At location No. 6, in particular, four thermocouples were placed around the tube wall. The result was that no difference was detected between their indications.

3.2. *Experimental results*

Figure 18 shows measured Nusselt number against $Re\,Ra$ with De as a parameter. These results agree with the numerical prediction within 30%. A trend that the experimental results are less than the numerical ones is found in the figure. This may be attributed to underestimating of the outlet temperature due to a loss of heat from the mixing cup and/or a thermal resistance due to air bubbles attached to the tube wall.

4. CONCLUSION

There is a composite region of heat transfer in a helically coiled tube in which both the centrifugal and buoyancy forces are significant. Equations (28) and (29) give its boundaries if De and $Re\,Ra$ are replaced by $De\cos\alpha$ and $Re\,Ra\cos\alpha$, respectively. The Nusselt number in this region can be regarded as a function of $De\,Pr^{0.54}\cos\alpha$ and $Re\,Ra\,Pr\cos\alpha$ alone, so long as the inclination angle α is not very large. Equation (30) gives an approximate expression for this Nusselt number.

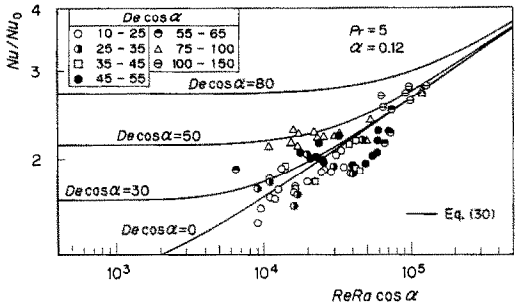

FIG. 18. Experimental results and a comparison with equation (30).

Acknowledgement—The authors express their thanks to Prof. K. Mizukami of Ehime University for looking over the manuscript and making valuable comments.

REFERENCES

1. Y. Mori and W. Nakayama, Study on forced convective heat transfer in curved pipes (1st report, laminar region), *Int. J. Heat Mass Transfer* **8**, 67–82 (1965).
2. R. A. Seban and E. F. McLaughlin, Heat transfer in tube coils with laminar and turbulent flow, *Int. J. Heat Mass Transfer* **6**, 387–395 (1963).
3. M. Akiyama and K. C. Cheng, Boundary vorticity method for laminar forced convection heat transfer in curved pipes, *Int. J. Heat Mass Transfer* **14**, 1659–1675 (1971).
4. A. N. Dravid, K. A. Smith, E. W. Merrill and P. L. T. Blian, Effect of secondary fluid motion on laminar flow heat transfer in helically coiled tubes, *A.I.Ch.E. Jl* **17**, 1114–1122 (1971).
5. L. A. M. Janssen and C. J. Hoogendoorn, Laminar convective heat transfer in helical coiled tubes, *Int. J. Heat Mass Transfer* **21**, 1197–1206 (1978).

6. C. E. Kalb and J. D. Seader, Heat and mass transfer phenomena for viscous flow in curved circular tubes, *Int. J. Heat Mass Transfer* **15,** 801–817 (1972).
7. Z. Zapryanov, Ch. Christov and E. Toshev, Fully developed laminar flow and heat transfer in curved tubes, *Int. J. Heat Mass Transfer* **23,** 873–880 (1980).
8. S. V. Patanker, V. S. Pratap and D. B. Spalding, Prediction of laminar flow and heat transfer in helically coiled pipes, *J. Fluid Mech.* **62,** 539–551 (1974).
9. G. J. Hwang and K. C. Cheng, Boundary vorticity method for convective heat transfer with secondary flow—application to the combined free and forced laminar convection in horizontal tubes, *Heat Transfer 1970,* Vol. 4, NC 3.5. Elsevier, Amsterdam (1970).
10. K. Futagami and H. Abe, Forced-natural combined convective heat transfer in inclined straight tubes (1st report, laminar region), *Trans. J.S.M.E.* **38,** 1799–1811 (1972) (in Japanese).
11. M. Akiyama, M. Suzuki, K. C. Cheng, M. Suzuki and I. Nishiwaki, Mixed convection problems in the entrance region of curved circular tubes, *Trans. J.S.M.E.* **50,** 1197–1204 (1983) (in Japanese).
12. J. Prusa and L. S. Yao, Numerical solution for fully developed flow in heated curved tubes, *J. Fluid Mech.* **123,** 503–522 (1982).
13. J. B. Lee, H. A. Simon and J. C. F. Chow, Buoyancy in laminar curved tube flows, ASME–JSME Thermal Engineering Joint Conference 1983, Vol. 3, pp. 133–139 (1983).
14. S. P. N. Singh and K. J. Bell, Laminar flow heat transfer in a helically-coiled tube, *Heat-Transfer 1974,* Vol. 2, pp. 193–197 (1974).
15. K. Futagami, Y. Aoyama and H. Abe, Laminar heat transfer in a helically coiled tube, *Trans. J.S.M.E.* **47,** 1995–2003 (1981) (in Japanese).
16. A. D. Gosman, W. M. Pun, A. K. Runchal, D. B. Spalding and M. Wolfshtein, *Heat and Mass Transfer in Recirculating Flow,* Section 3.23. Academic Press, New York (1969).
17. A. D. Gosman, W. M. Pun, A. K. Runchal, D. B. Spalding and M. Wolffshtein, *Heat and Mass Transfer in Recirculating Flow,* pp. 115–116. Academic Press, New York (1969).
18. P. J. Roache, *Computational Fluid Dynamics,* pp. 141–142. Hermosa, Albuquerque, New Mexico (1976).
19. Y. Mori and K. Futagami, Forced convective heat transfer in uniformly heated horizontal tubes (2nd report, theoretical study), *Int. J. Heat Mass Transfer* **10,** 1801–1813 (1967).
20. H. Ito, Laminar flow in curved pipes, *ZAMM* **49,** 653–663 (1969).

TRANSFERT THERMIQUE LAMINAIRE DANS UN TUBE EN SERPENTIN

Résumé—Une étude théorique et expérimentale concerne l'effet de l'écoulement secondaire sur le transfert thermique entre un serpentin chauffé uniformément et l'écoulement laminaire établi. On prend en compte les forces centrifuges et de pesanteur dans l'analyse numérique. Les solutions couvrent un large domaine de nombre de Prandtl. On obtient les profils de vitesse et de température, le coefficient de frottement et le coefficient de transfert. Les effets de l'écoulement secondaire sur le transfert thermique sont divisés en trois classes : ceux dans le domaine centrifuge, ou flottant ou mixte ; les frontières sont précisées. Une expression approchée pour le nombre de Nusselt moyen sur la périphérie est donnée en fonction de deux facteurs simples. Une comparaison est faite avec les résultats des expériences utilisant l'eau. On discute l'effet de l'inclinaison du tube.

WÄRMEÜBERGANG BEI LAMINARER STRÖMUNG IN ROHRWENDELN

Zusammenfassung—Der Einfluß der Sekundärströmung auf den Wärmeübergang von einem gewendelten, gleichmäßig beheizten Rohr an eine vollständig ausgebildete Laminarströmung wurde experimentell und theoretisch untersucht. In der numerischen Untersuchung werden sowohl Zentrifugal- als auch Auftriebskräfte berücksichtigt. Geschwindigkeits- und Temperaturprofile, Reibungsbeiwert und Wärmeübergangskoeffizient wurden für einen weiten Bereich der Prandtl-Zahl berechnet. Der Einfluß der Sekundärströmung auf den Wärmeübergang wurde in drei Bereiche aufgeteilt, einen zentrifugalen, einen auftriebsbedingten und einen mit beiden überlagerten. Die Grenzen zwischen den Bereichen wurden bestimmt. Eine Näherungsbeziehung für die über den Umfang gemittelte Nusselt-Zahl im überlagerten Bereich wird als Funktion zweier einfacher Faktoren angegeben. Die Ergebnisse werden mit Messungen mit Wasser verglichen, und der Einfluß der Steigung des Rohres wird diskutiert.

ЛАМИНАРНЫЙ ТЕПЛООБМЕН В СПИРАЛЬНО ЗАКРУЧЕННОЙ ТРУБЕ

Аннотация—Теоретически и экспериментально исследовано влияние вторичного течения на теплоотдачу от равномерно нагретой спирально закрученной трубы в полностью развитом ламинарном потоке. В численном анализе учитываются центробежные и подъемные силы. Расчеты проводятся в широком диапазоне чисел Прандтля. Получены профили скорости и температуры, коэффициенты трения и теплообмена. Влияние вторичных течений на теплоотдачу делится на три типа: области превалирующего влияния либо подъемных, либо центробежных сил и смешанная область; определены границы областей. Представлено приближенное выражение для осредненного по периметру числа Нуссельта в смешанной области как функции двух простых факторов. Проведено сравнение с результатами экспериментов для воды. Обсуждается влияние наклона трубы.